



HAL
open science

Plasmons in Graphene Nanostructures with Point Defects and Impurities

François Aguillon, Dana Codruta Marinica, Andrey Borissov

► **To cite this version:**

François Aguillon, Dana Codruta Marinica, Andrey Borissov. Plasmons in Graphene Nanostructures with Point Defects and Impurities. *Journal of Physical Chemistry C*, 2021, 125 (39), pp.21503-21510. 10.1021/acs.jpcc.1c05182 . hal-03355820

HAL Id: hal-03355820

<https://hal.science/hal-03355820v1>

Submitted on 27 Sep 2021

HAL is a multi-disciplinary open access archive for the deposit and dissemination of scientific research documents, whether they are published or not. The documents may come from teaching and research institutions in France or abroad, or from public or private research centers.

L'archive ouverte pluridisciplinaire **HAL**, est destinée au dépôt et à la diffusion de documents scientifiques de niveau recherche, publiés ou non, émanant des établissements d'enseignement et de recherche français ou étrangers, des laboratoires publics ou privés.

Plasmons in Graphene Nanostructures with Point Defects and Impurities

François Aguilon, Dana Codruta Marinica, and Andrei G. Borisov*

*Institut des Sciences Moléculaires d'Orsay, UMR 8214, CNRS, Université Paris-Saclay,
Bâtiment 520, 91405 Orsay Cedex, France*

E-mail: andrei.borisov@universite-paris-saclay.fr

Phone: +33 (0)1 69157697

Abstract

The exceptional electronic and optical properties of graphene are harmed by the unavoidable imperfections of the lattice resulting from mechanical or electronic interaction with the environment. Using a time dependent approach we theoretically address the sensitivity of the plasmon modes of graphene nanoflakes to the presence of point vacancy defects and substitutional impurities. We find that the fractions of the defects as low as 10^{-3} from the total number of Carbon atoms in an ideal nanoflake lead to strong broadening of the plasmon resonance in the optical absorption spectrum. In addition to this effect resulting from the elastic and inelastic processes associated with defect induced scattering and modification of the electronic structure of graphene, we also observe and explain a vacancy and impurity induced shifts of the plasmon energy. Our work extends the in depth theoretical studies of the optical properties of graphene nanomaterials towards practical situations of nonideal 2D lattices.

Introduction

Graphene and other 2D materials offer unprecedented opportunities in various fields of nanotechnology such as electronics, optoelectronics, and nanosensors among others.^{1,2} High carrier mobility, possibility to tune the optical response with doping, strong confinement of plasmonic fields, and high nonlinear response placed graphene and graphene nanostructures at the focus of experimental and theoretical studies over past years.³⁻⁵ Meanwhile, the performance of the actual devices is far from the theoretically estimated possibilities, in particular because the inevitable defects and impurities act as efficient scatterers for the 2D electrons thus degrading the electron transport properties of graphene and its plasmon response.⁶⁻¹⁰

The effect of the point defects and impurities on the electronic structure and transport in graphene has been thoroughly studied in the context of the dc electron transport.^{6,7,9,11-15} It has been demonstrated that the associated scattering of the 2D electrons decreases the dc conductivity through the decrease of the transport scattering time. In the context of the time varying fields, using the Drude theory,^{16,17} one concludes on increased attenuation and corresponding broadening of the plasmon resonances in graphene nanostructures. Moreover, the presence of defects such as nanoparticle boundary leads to the plasmon decay via an electron hole pair creation (Landau damping mechanism).^{8,18-20} These considerations probably explain the lack of the studies of the plasmon resonances in graphene nanostructures with nonideal lattice. Indeed, most of the effort concentrated on the exceptional perspectives offered by graphene plasmonics, while the increased attenuation of the plasmon resonance harms performance of the devices. Nowadays however, an increased interest in controlling electronic properties of graphene with impurities²¹⁻²³ naturally puts a question of an associated impurity effect on the plasmon modes.

In this work, using a time-dependent tight-binding approach we study how the atomic vacancy defects and impurities affect the plasmon modes and optical response of graphene nanostructures doped to a fixed Fermi energy via e.g. electrical gating. We find that defect

fractions as low as one per thousand lattice atoms lead to an appreciable broadening, and, in certain cases, to the quenching of the plasmon resonance in the absorption spectra. Simultaneously we obtain a shift of the plasmon energy. While the former result is consistent with impurity scattering mechanism leading to the plasmon decay, the shift of the plasmon energy stems from the change of the density of electronic states at the Fermi level.

Unless otherwise stated atomic units are used throughout the paper.

Methods

To follow the dynamics of charges induced in ideal and defected graphene nanoflakes by an incident electromagnetic radiation, we use the real-time formulation of the tight-binding Hartree approach to graphene plasmonics developed by García de Abajo and collaborators in Ref. 18 and later in Ref. 24. The details on our time dependent tight binding (TDTB) method can be found elsewhere.²⁵ In brief, the occupied electron orbitals of the graphene nanoflake are sought in the form

$$\psi_j(\mathbf{r}, t) = \sum_{\ell} \tilde{\psi}_{j\ell}(t) \varphi_{2p}(\mathbf{r} - \mathbf{r}_{\ell}), \quad (1)$$

where $\varphi_{2p}(\mathbf{r} - \mathbf{r}_{\ell})$ is the wave function of the $2p_z$ -orbital centered at a Carbon lattice site ℓ . The time-dependence of the vector of coefficients $\tilde{\psi}_j(t) = \begin{bmatrix} \tilde{\psi}_{j1}(t) \\ \vdots \\ \tilde{\psi}_{jN}(t) \end{bmatrix}$, where N stands for the number of carbon atoms in the nanostructure, is given by the time-dependent Schrödinger equation

$$i\partial_t \tilde{\psi}_j(t) = \mathbb{H}[\delta n(t)] \tilde{\psi}_j(t). \quad (2)$$

The tight-binding Hamiltonian of the system, \mathbb{H} , depends on the field-induced changes of the diagonal elements of the density matrix $n_{\ell}(t)$ given by

$$\delta n_{\ell}(t) = n_{\ell}(t) - n_{\ell}(t=0) = 2 \sum_{j=\text{occ}} \left\{ \left| \tilde{\psi}_{j\ell}(t) \right|^2 - \left| \tilde{\psi}_{j\ell}(t=0) \right|^2 \right\}, \quad (3)$$

where $-\delta n_\ell$ corresponds to the electron charge induced at site ℓ . The sum in equation Eq. 3 runs over all occupied orbitals with energies $E_j \leq E_F$. The occupied ground-state orbitals, $\tilde{\psi}_{j\ell}(t=0)$, and their energies, E_j , are obtained by diagonalization of the Hamiltonian matrix (defined below) in the absence of the external perturbation, and considering that the graphene nanostructure is doped by electrical gating to a fixed Fermi energy E_F . For an insulated neutral structure without vacancy defects or impurities, $E_F = 0$.

The matrix elements, $H_{\ell\ell'}$, of the tight-binding Hamiltonian are given by

$$\begin{aligned} H_{\ell\ell'} &= h\Theta(|\mathbf{r}_\ell - \mathbf{r}_{\ell'}|), \quad \text{if } \ell \neq \ell', \\ H_{\ell\ell} &= V_{\text{ext}}(\mathbf{r}_\ell, t) + \mathcal{U}_{\text{on}}\delta n_\ell + \sum_{\ell'} \frac{\delta n_{\ell'}}{|\mathbf{r}_{\ell'} - \mathbf{r}_\ell|}, \end{aligned} \quad (4)$$

where the hopping matrix elements $h = -2.8$ eV;³ the cutoff function $\Theta(r) = 1$ for the nearest neighbours ($r = 1.42$ Å) and $\Theta(r) = 0$ otherwise. The time-dependent potential created by an incident laser pulse at the carbon lattice site ℓ is denoted as $V_{\text{ext}}(\mathbf{r}_\ell, t)$. Finally, the on-site interaction $\mathcal{U}_{\text{on}} = 0.58$.¹⁸

Because of the small size of the systems considered in this study, the retardation effects and the radiative decay of the plasmon modes are neglected. We thus focus this study on the broadening of the localized plasmon resulting from the elastic and inelastic processes induced by the defects and impurities such as e.g. the reduction of the collision transport time^{13-16,26} or Landau damping associated with plasmon energy transfer to electron hole pair excitations.^{8,10,18-20,27,28} Inline with simple yet representative and widely used approaches, the point defects are modeled removing N_i carbon atoms at randomly chosen lattice sites,^{6,11,14,29} which is of course an approximation to the complex realistic situation.³⁰ Similarly, the substitutional impurities located at N_i randomly chosen lattice sites $\{\ell_1, \ell_2, \dots, \ell_{N_i}\}$ are modeled by adding the $U \sum_{k=1}^{N_i} \delta_{\ell_k\ell}$ term ($\delta_{\ell_k\ell}$ is the Kronecker delta) to the Hamiltonian matrix element $H_{\ell\ell}$ given by Eq. 4.^{11,31-33} The impurity potential U represents the energy shift of the impurity p_z orbital with respect to the p_z orbital of the Carbon atom.

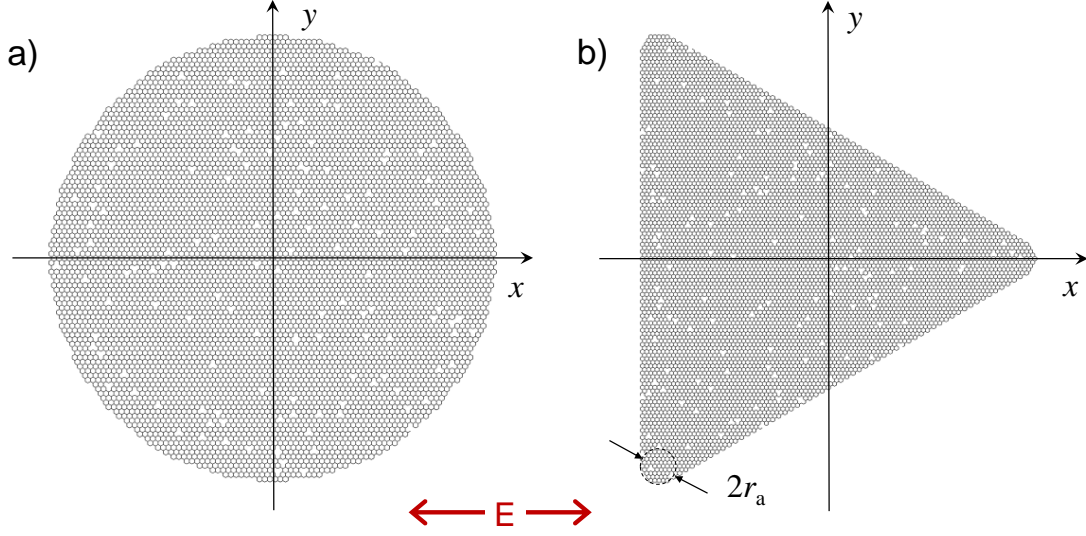


Figure 1: Sketch of the atomistic structure of the circular (**panel a**) and triangular (**panel b**) graphene nanoflakes comprising $N_a = 13452$ (circular) and $N_a = 13458$ (triangular) atoms in an ideal (no defects) lattice. The tips of the triangle are made smooth with curvature radii $r_a = 1$ nm. For each nanoflake, the vacancy defects are modelled removing carbon atoms at N_i randomly distributed lattice sites. Therefore, the vacancy defects appear in panels **a** and **b** as white dots within the carbon lattice. For the situation presented here, the vacancy fraction is $\mathcal{C}_i = N_i/N_a = 10^{-3}$. The calculations of the optical response are performed considering an incident electromagnetic plane wave with an electric field \mathbf{E} , and linear polarisation along the x -axis as indicated with double red arrow.

As representative examples of graphene nanoantennas supporting dipolar plasmon modes we consider nanoflakes of circular and equilateral triangle shape cut from an ideal graphene plane as shown in Fig. 1. The carbon atoms with single neighbor are removed at the borders. For the triangular nanoantennas we set the geometry such that edges are armchair leading to the lower edge scattering and thus better defined plasmon modes. The tips of the triangle have curvature radii ($r_a = 1$ nm). Throughout the paper we use the coordinate system where the z -axis is perpendicular to graphene plane and y - and x - axes are in-plane. For the optical response calculations, the incident electromagnetic plane wave is linearly polarized with electric field vector $\mathbf{E}(t)$ oscillating along the x -axis. Thus, $\mathbf{E}(t) = \hat{e}_x E(t)$, where \hat{e}_x is the unit length vector in positive x -direction, so that the external potential can be expressed as $V_{\text{ext}}(\mathbf{r}_\ell, t) = E(t) \hat{e}_x \cdot \mathbf{r}_\ell$.

Results

The absorption spectra calculated for circular graphene nanoflakes of radii $R_{cl} = 7.47$ nm and $R_{cl} = 10.6$ nm, comprising respectively $N_a = 6690$ and $N_a = 13452$ carbon atoms in defect-free case, are shown in Figure 2 for various fractions of the carbon atom vacancies \mathcal{C}_i . The vacancy fraction is defined as $\mathcal{C}_i = N_i/N_a$, where N_i is the number of vacancies introduced at random positions in the nanoflake. For the sake of comparison with earlier publication,²⁵ we show here the results obtained with nanoparticles doped to the Fermi energy $E_F = 0.36$ eV as measured with respect to the $E = 0$ Dirac energy point of an ideal nanoflake. Below in this work we also show the results obtained with $E_F = 0.6$ eV. This level of doping is typically used in the theoretical and experimental works on graphene plasmonics addressing the infrared spectral region.^{4,24,34–36}

Without defects, the adsorption spectrum is dominated by the dipolar plasmon (DP) resonance which shifts to lower energy for the larger size nanoflake inline with predictions of the analytical approach developed within the nonretarded approximation.^{4,36} The width of the associated absorption resonance in this case reflects the rate of the plasmon decay via electron-hole excitations (Landau damping) because of the scattering at the edges of the structure. With increasing number of vacancies, the defect induced elastic scattering of conduction electrons,^{8,14,16,17,20} and the energy exchange between plasmon and electron hole pair excitations involving the inter-band transitions between the π bands of graphene and defect induced states^{10,20,27,28} lead to the increase of the plasmon decay rate. As a consequence, the DP resonance feature in the absorption spectra strongly broadens and practically disappears for the defect fractions as low as 10^{-3} for the small nanoflake and 5×10^{-3} for the larger size nanoflake. We attribute the larger broadening obtained for the smaller nanoparticle to the interference between the point defect and boundary scattering. Indeed, analysing the electronic states of the nanoflake, we observe a strong hybridization between the vacancy induced states close to the Dirac point ($E = 0$) and the edge states.

Note that the TDTB approach does not allow one to account for plasmon decay channels

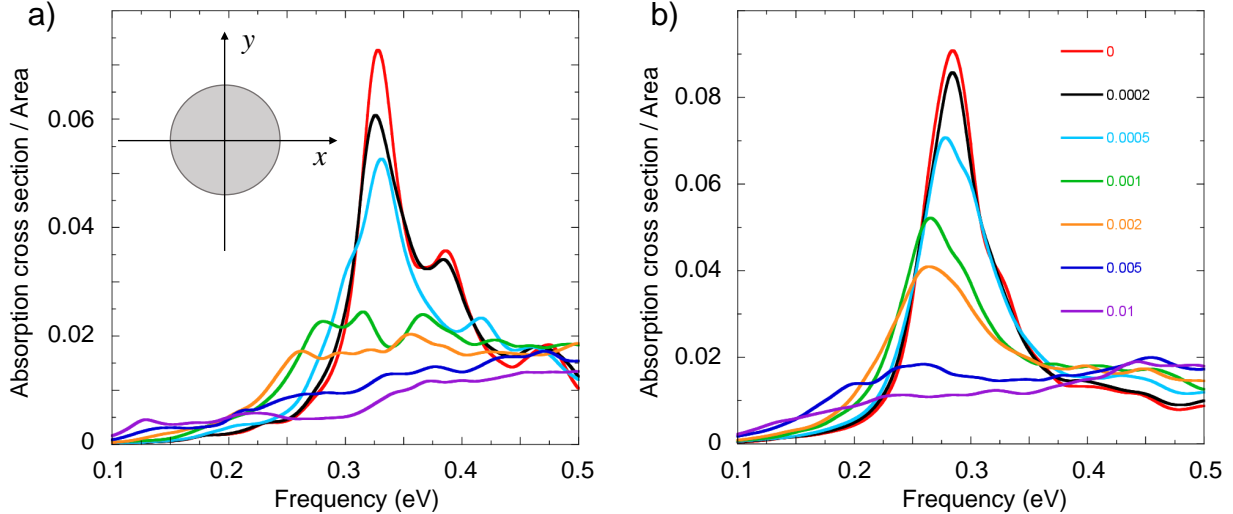


Figure 2: Analysis of the dipolar plasmon resonance in the optical response of circular graphene nanoflakes with vacancy defects. The insert of panel a sketches the geometry. The nanoflakes are doped to the Fermi energy $E_F = 0.36$ eV. The absorption spectra are artificially broadened by $\gamma_b = 15$ meV. **Panel a**: Absorption cross-section per unit area of the nanoflake with radius $R_{cl} = 7.47$ nm, comprising $N_a = 6690$ graphene atoms in an ideal lattice (defect-free case). Results are shown as function of the frequency of an incident x -polarized electromagnetic plane wave for various fractions of carbon vacancies $\mathcal{C}_i = N_i/N_a$, where N_i is the number of vacancies. The color code is explained in the legend. **Panel b**: The same as panel a but for the $R_{cl} = 10.6$ nm, $N_a = 13452$ nanoflake.

such as those related to the interaction with optical phonons. In particular, for the energies of the plasmon modes considered in this work that are above the optical phonon frequency (≈ 0.2 eV), the plasmon decay with excitation of the optical phonons in graphene can lead to an appreciable plasmon line broadening within 15 – 40 meV range.^{5,16,28} Following earlier studies,^{37,38} the absorption spectra calculated in this work are artificially broadened by γ_b to phenomenologically account for the role of the optical phonons. Within this phenomenological approach the defect-induced and phonon-induced decay channels provide additive contributions to the total plasmon line width. For the sake of presentation we use the lower bound, $\gamma_b = 15$ meV, so that the modifications of the absorption spectra are clearly visible for low defect fractions. For high defect fractions, the defect-induced broadening of the plasmon resonance is the dominating effect, as follows from Figure 2 and results discussed below in this work.

As another representative example of plasmonic graphene nanoantennas we consider triangular graphene flakes with armchair edges. The optical absorption spectra calculated with TDTB approach are shown in panels a,b,c of Figure 3 for two sizes of triangles ($N_a = 6666$ and $N_a = 13458$), and considering two values of doping corresponding to the Fermi energies $E_F = 0.36$ eV, and $E_F = 0.6$ eV. While the spectral changes with increasing defect fraction are similar to that discussed for circular geometry (Figure 2), their analysis is simplified in the present situation, owing to the smaller Landau damping and thus to the narrower plasmon resonance structure in the absorption spectra.

Comparing absorption spectra obtained with nanotriangles of different size and with two values of electron doping, one observes that the dipolar plasmon is blue-shifted with increasing E_F for the fixed size of the nanoflake, and it is red-shifted with increasing size of the nanoflake (fixed E_F) as expected considering the in-plane conductivity of graphene and the scaling of the plasmon mode frequency.^{4,36} Increasing \mathcal{C}_i leads to the broadening and disappearance of the plasmon resonance similar to the case of circular nanoflakes. For the larger E_F , however, the resonance feature in the absorption spectra persists up to higher defect fractions. Indeed, the vacancy defect induced changes in the electronic structure of graphene develop close to the Dirac point at low \mathcal{C}_i and progressively extend to higher energies with increasing \mathcal{C}_i .^{6,11-14} Therefore, higher level of electron doping, E_F , reduces the plasmon decay via the inelastic transitions involving the defect induced electronic states.^{10,17,27,28,39,40} Similar to the results obtained for the circular nanoflakes, increasing the size of the graphene nanoantenna for fixed doping reduces the edge effects and thus the Landau damping, and leads to the narrower resonant feature in the absorption spectra. Well developed plasmon modes of the triangular patches reveal an additional modification of the absorption spectra also seen for the larger circular nanoflake. Namely, along with broadening, the plasmon resonance red-shifts with increasing defect fraction \mathcal{C}_i .

Detailed analysis of the evolution of the width and of the frequency of the DP with \mathcal{C}_i is shown in Figure 3d for nanoparticles of different size, geometry and electron doping. In this

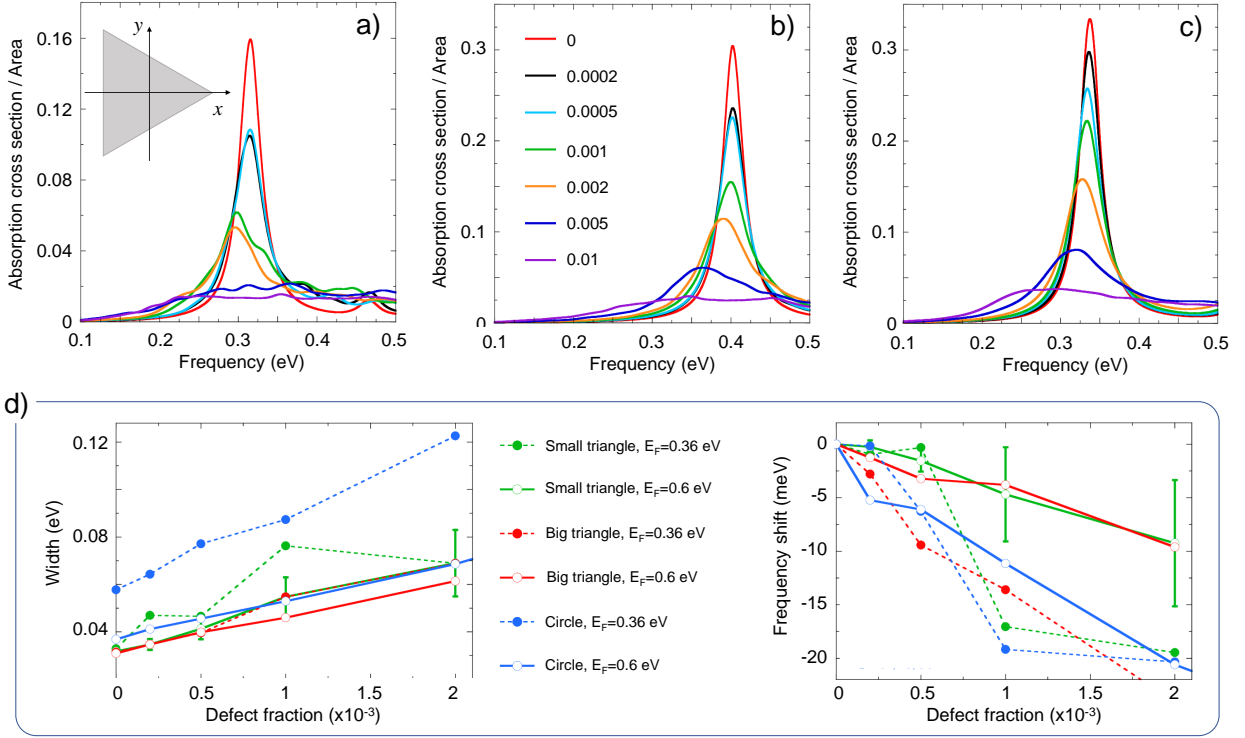


Figure 3: Analysis of the dipolar plasmon resonance in the optical response of triangular graphene nanoflakes with armchair boundary and vacancy defects. The insert of panel a sketches the geometry. **Panel a:** Absorption cross-section per unit area of the (small) nanoflake comprising $N_a = 6666$ carbon atoms in the defect-free case. The nanoparticle is doped to a Fermi energy $E_F = 0.36$ eV. Results are shown as function of the frequency of an incident x -polarized plane wave for different vacancy fractions C_i . The color code is explained in the legend of panel b. **Panel b:** The same as panel a, but for $E_F = 0.6$ eV. **Panel c:** The same as panel a, but for the (large) $N_a = 13458$, $E_F = 0.6$ eV triangular nanoflake. **Panel d:** The width Γ_{DP} and the frequency shift $\omega_{DP} - \omega_{DP}^0$, of the dipolar plasmon resonance as function of the defect fraction C_i . Here ω_{DP} is the frequency of the absorption resonance at finite defect fraction, and ω_{DP}^0 is the frequency of the absorption resonance of an ideal nanoflake. Results are shown for the triangular ($N_a = 6666$, $N_a = 13458$) and for the circular ($N_a = 13452$) graphene nanoflakes and for various values of E_F as explained in the insert. For the $N_a = 6666$, $E_F = 0.6$ eV triangular graphene nanoflake with error bars we show the statistical dispersion of the results obtained with 10 random samples of the defect positions.

figure we focus on the range of small C_i , so that the plasmon mode is well defined, meaning $\Gamma \ll \omega_{DP}$. Here Γ and ω_{DP} are respectively the width and the frequency of the plasmon resonance. Because of the computational restrictions, the results are obtained using single random sample of the defects, except for the $N_a = 6666$, $E_F = 0.6$ eV triangle. In this latter case, the dispersion of the results with defect positions was studied using 10 random samples

of the defects within the nanoflake. As a result, despite the fact that a rather large statistical dispersion of the results might be expected, robust general trends emerge. We obtain that with increasing vacancy fraction (i) the width Γ of the plasmon resonance linearly increases, while (ii) the plasmon frequency ω_{DP} features a red-shift. The offset of the $\Gamma(\mathcal{C}_i)$ dependence is different for different nanostructures reflecting at $\mathcal{C}_i = 0$ the Landau damping because of the nanoflake boundary. At the same time, the slope of $\Gamma(\mathcal{C}_i)$ is very similar for all the cases addressed here. At variance, the plasmon frequency is less sensitive to the defects for the triangular nanoflakes with higher E_F . Note however, that the plasmon coupling with electron-hole pair excitations^{41,42} might lead to the non-Lorentzian profile of the resonance in the adsorption spectrum (see e.g. Figure 2a and Figure 3a, $\mathcal{C}_i = 0.001$) which is difficult to analyse. Along with statistical dispersion, this explains the non-monotonous character of the results obtained in certain cases.

Discussion

The calculated modification of the DP mode of graphene nanoflakes by the vacancy defects can be understood using the Drude model for in-plane conductivity,^{4,5,15,16,43} and the theory of the non-retarded plasmons in graphene nanostructures.^{4,36} Within the Drude model, the ac conductivity of the electrostatically doped graphene is given by

$$\sigma(\omega) = \frac{v_f^2}{2} \rho(E_F) \frac{\tau(\omega)}{1 - i\omega\tau(\omega)}, \quad (5)$$

where $\rho(E_F)$ is the density of electronic states (DOS) at the Fermi level, v_f is the Fermi velocity of graphene, and $\tau(\omega)$ is the ac relaxation time^{39,40} given by several contributions including elastic collisions with defects ($\tau_{\text{el}} \propto \mathcal{C}_i^{-1}$, as follows from the semiclassical transport theory^{6,14,15}). Considering that $\rho(E_F)$ is given by that of a doped ideal graphene, $\rho(E_F) = \frac{2|E_F|}{\pi v_f^2}$, one obtains $\sigma(\omega) = \frac{|E_F|}{\pi} \frac{\tau(\omega)}{1 - i\omega\tau(\omega)}$.

The non-retarded analysis of the plasmon resonances in small graphene nanostructures^{4,35,36}

allows the plasmon eigenmode expansion of the polarizability, $\alpha(\omega)$, of the nanoflake. Retaining only the dipolar plasmon mode for the free-standing graphene nanoflake with characteristic size D

$$\alpha(\omega) = D^3 \frac{A}{\xi - i\omega D/\sigma(\omega)}, \quad (6)$$

where A and ξ are real positive constants defined by the geometry of the system. Using Eq. 5 we obtain close to the DP resonance

$$\alpha(\omega) = D^2 A \frac{\omega_p^2}{\omega_{\text{DP}}^2 - \omega(\omega + i\Gamma)}, \quad (7)$$

where $\omega_p = \sqrt{\frac{v_f^2}{2}\rho(E_F)}$ is an analogue of the plasma frequency for metal nanoparticles, and the frequency of the DP

$$\omega_{\text{DP}} = \omega_p \sqrt{\frac{\xi}{D}}, \text{ i.e. } \omega_{\text{DP}} \propto \sqrt{\rho(E_F)/D}. \quad (8)$$

Note that the position of the absorption maximum is shifted with respect to the frequency of the DP, ω_{DP} , by a small amount $\simeq \Gamma^2$, which is neglected in our discussion of the results. Using the expression for DOS of an ideal graphene leads to $\omega_{\text{DP}} \propto \sqrt{|E_F|/D}$ which explains the difference in plasmon energies of the defect-free nanoparticles with different size (D) and doping (E_F).

In defining the polarizability of the graphene nanoflake (Equation 7) we introduced an effective attenuation of the DP mode $\Gamma = \gamma_L + \gamma_i + \gamma_b$ which accounts for the plasmon resonance broadening because of several contributions. (i) The Landau damping at the boundaries of the nanostructure (rate γ_L). (ii) The defect or impurity induced elastic and inelastic scattering (rate γ_i). (iii) Other mechanisms such as phonon scattering introduced phenomenologically by an artificial broadening γ_b of the calculated absorption spectra. These contributions to Γ are witnessed by Figure 3d, which shows at $\mathcal{C}_i = 0$ a geometry dependent contribution related to γ_L , larger for the circular nanoflakes (which have large portions

of zigzag edges) than for the triangular ones (which have armchair edges), and a linear dependence of γ_i with respect to \mathcal{C}_i , which roughly speaking is the same for any nanoflake geometry.

As follows from Equation 8, the frequency of the DP is determined by the density of electronic states at the Fermi level, $\rho(E_F)$. For low defect fractions $\mathcal{C}_i \lesssim 10^{-3}$, the DOS $\rho(E_F)$ decreases with increasing \mathcal{C}_i as we calculate here in agreement with earlier reports. This explains the red-shift of the DP frequency with increasing \mathcal{C}_i .^{11-15,44} It is worth mentioning that $\rho(E_F)$ sharply increases at high \mathcal{C}_i ^{11,12} reflecting evolution of the spectra owing to the vacancy induced states close to the Dirac point. However, at these high defect fractions the plasmon modes are extremely broadened by the defect scattering so that the ω_{DP} cannot be defined in any case.

While the modification of the density of electronic states $\rho(E_F)$ with \mathcal{C}_i is rather complex in the case of atomic vacancy defects, it takes a particular intuitive form for the model representation of the substitutional impurities in graphene lattice. As we discussed in the section devoted to the method, the representative yet simple model of impurities consists in considering the change of the p_z electron energy level at impurity site. This is accounted for by adding the impurity potential U at the corresponding position at the diagonal of the tight-binding Hamiltonian matrix. In this situation, at low fractions of donor ($U < 0$, e.g. Nitrogen) or acceptor ($U > 0$, e.g. Boron) substitutional impurities, the modification of the band structure of graphene close to the Dirac point can be represented by a translation along the energy axis by $\Delta E \simeq \mathcal{C}_i U$ ^{11,45} as supported by ab initio calculations.²¹ For the doping of graphene with e.g. electrical gating that fixes E_F , as used here, and for small ΔE , the electron density of states at the Fermi level can be then expressed as

$$\rho(E_F) = \frac{2(E_F - \mathcal{C}_i U)}{\pi v_f^2}, \quad (9)$$

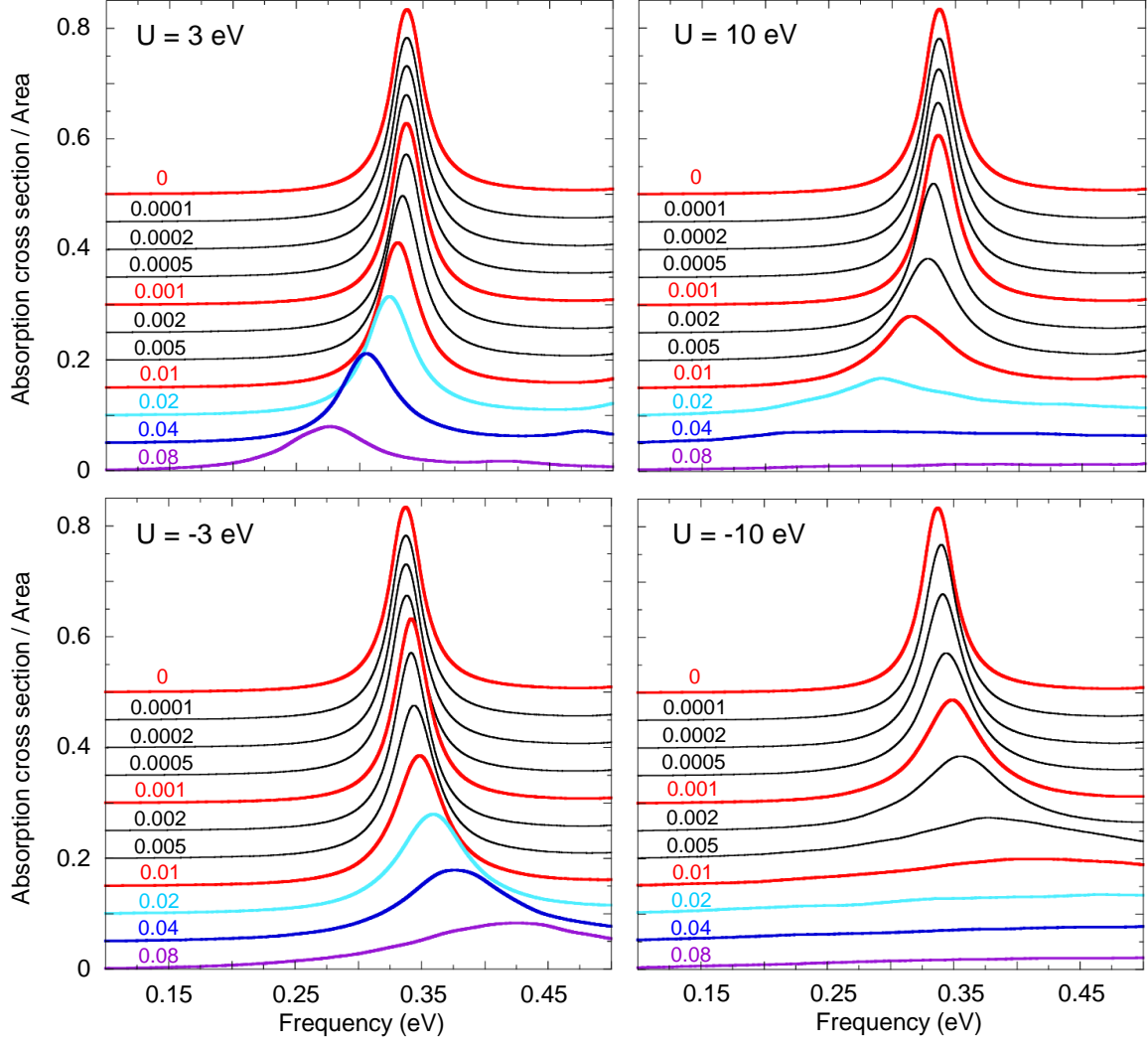


Figure 4: The effect of the substitutional impurities on the dipolar plasmon of the triangular graphene nanoflake with $N_a = 13548$ carbon atoms and armchair boundary. The nanoflake is doped to a Fermi energy $E_F = 0.6$ eV as measured from the Dirac point of an ideal (no impurities) nanoflake. **Panels:** Absorption cross-section per unit area as function of the frequency of an incident x -polarized plane wave for different impurity fractions $\mathcal{C}_i = N_i/N_a$, where N_i is the number of substitutional impurities introduced at random positions in the nanoflake. The TDTB calculations are performed for an impurity potential $U = \pm 3$ eV, ± 10 eV as indicated at corresponding panels. The color lines are labelled according to \mathcal{C}_i .

leading to the dipolar plasmon frequency

$$\frac{\omega_{\text{DP}} - \omega_{\text{DP}}^0}{\omega_{\text{DP}}^0} \approx -\frac{\mathcal{C}_i U}{2E_F}, \quad (10)$$

where ω_{DP}^0 is the DP frequency of an ideal graphene nanoflake. Thus, for positive (negative) impurity potential U one expects a red-shift (blue-shift) of the DP frequency. Note that in the absence of external gating the impurities will determine the E_F energy relative to the Dirac point via number of p electrons injected or removed from the π band of graphene. We discuss this situation in Supporting Information.

The theoretical prediction of the DP frequency dependence on \mathcal{C}_i and U is fully supported by the TDTB results shown in Figure 4. The absorption spectra calculated for the $N_a = 13548$, $E_F = 0.6$ eV triangular nanoflake for various \mathcal{C}_i display red-shift (blue-shift) and broadening of the DP resonance with increasing fraction of the impurities with positive (negative) U . As in the carbon vacancies case, the broadening of the plasmon peak can be associated to the opening of new decay and dephasing channels because of the impurity scattering and impurity-induced electronic states. Larger impurity potential $|U|$ is producing larger effect with DP resonance disappearing in the absorption spectra calculated with $U = 10$ eV (-10 eV) for $\mathcal{C}_i = 0.08$ (0.02). Note that in this case the DP resonance persist up to larger disorder as compared to the vacancy defects.

In Figure 5 we further analyse the TDTB results obtained for the $N_a = 13548$, $E_F = 0.6$ eV triangular graphene nanoantenna with substitutional impurities. Similar to the vacancy defects, for the $U = 3$ eV case, we evaluated the statistical dispersion of the results performing calculations with 10 random samples of the impurity positions. Very small dispersion is obtained, justifying the use of a single random sample of impurities for the rest of the data.

The change of the DOS at the Fermi level, $\Delta\rho(E_F)$, is shown in Figure 5a. For small impurity potentials, and in agreement with theoretical predictions outlined above, $\rho(E_F)$ is a linear function of \mathcal{C}_i with its slope proportional to $-U$. With increasing $|U|$ however, even though the linearity dependence on \mathcal{C}_i is preserved within the range of impurity fractions studied here, the asymmetry between $\pm U$ results sets in with negative U leading to stronger effect on electronic density of states (see the results obtained with $U = \pm 10$ eV). This can

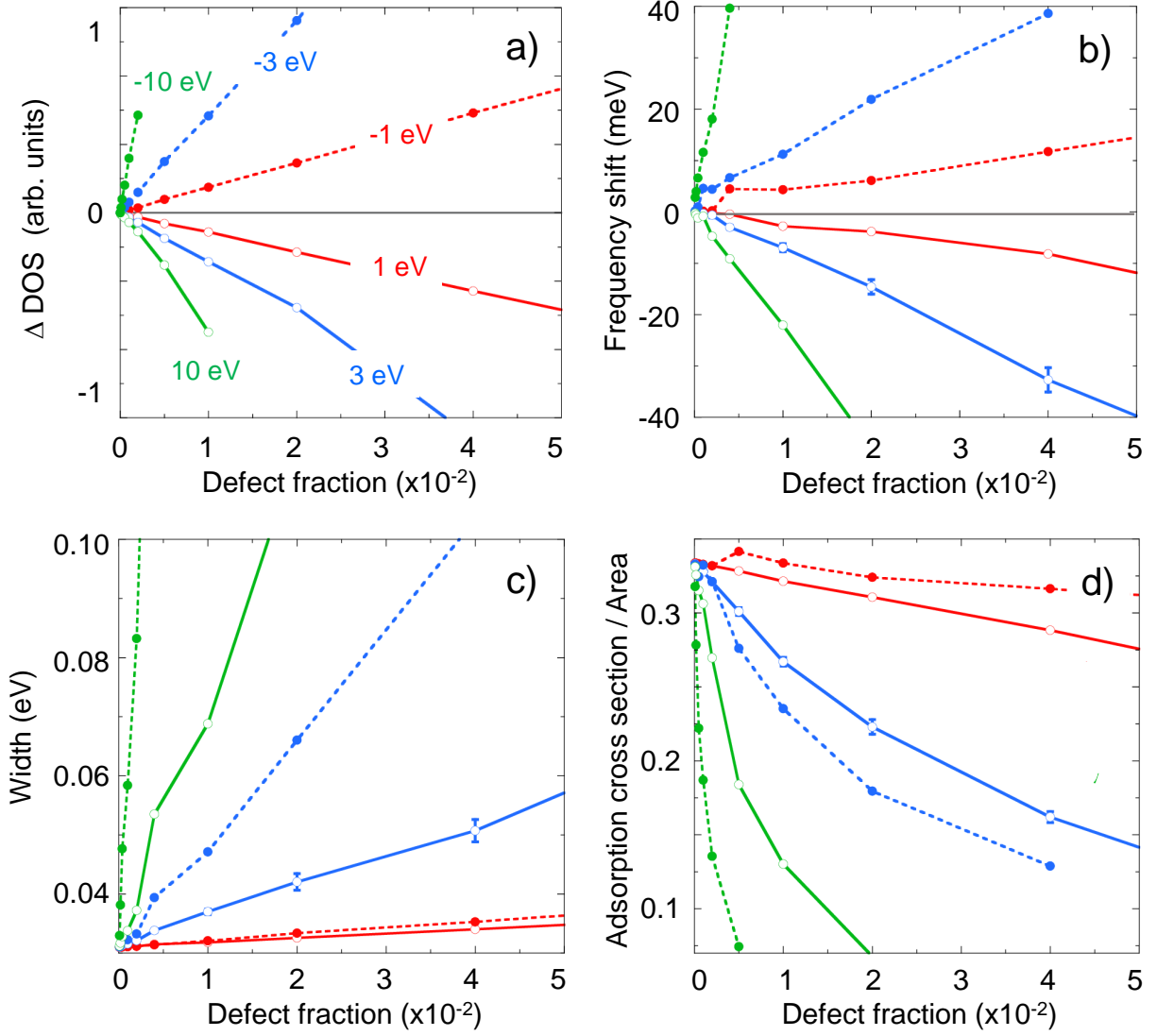


Figure 5: The effect of the impurities on plasmonic modes of the triangular $N_a = 13548$, $E_F = 0.6$ eV graphene nanoflakes with armchair boundary. Results for the negative (donor) and positive (acceptor) impurity potential U are shown as function of the impurity fraction. For each U the maximum \mathcal{C}_i is determined by the presence of the well-defined plasmon resonance in the absorption spectrum (see Figure 4). For the $U = 3$ eV case, with error bars we show the statistical dispersion of the results obtained with 10 random samples of the impurity positions. **Panel a:** Calculated change of DOS at the Fermi level, $\rho(E_F)$. The results are labeled according to the impurity potential U . **Panel b:** The frequency shift, $\omega_{\text{DP}} - \omega_{\text{DP}}^0$, of the dipolar plasmon resonance in absorption spectra. Here ω_{DP}^0 is the DP frequency of an ideal nanoflake. **Panel c:** The width, Γ_{DP} , of the dipolar plasmon resonance in absorption spectra. **Panel d:** The maximum absorption cross section measured at ω_{DP} .

be explained by the role of the impurity-induced resonances in DOS emerging below (above) the Dirac point for positive (negative) U ,^{11,33,45,46} thus affecting the $\rho(E_F)$ in a different way for positive or negative U .

The calculated change of the DP resonance frequency (Figure 5b) closely follows the results obtained for the change of the electronic density of states in agreement with trends predicted by Equation 8 and Equation 10. Thus, the $\omega_{\text{DP}} - \omega_{\text{DP}}^0$ shows a linear dependence on \mathcal{C}_i with blue (red) shift of ω_{DP} for positive (negative) U . Similar to $\rho(E_F)$, while $[\omega_{\text{DP}} - \omega_{\text{DP}}^0]_{|U=-1 \text{ eV}} \approx -[\omega_{\text{DP}} - \omega_{\text{DP}}^0]_{|U=1 \text{ eV}}$, the clear asymmetry between the results obtained with positive and negative U sets in at larger impurity potentials. Larger DP frequency shifts are obtained for the negative U .

The dependence of the width, Γ_{DP} , of the DP resonance in the absorption spectra on the impurity fraction, \mathcal{C}_i , is shown in Figure 5c for different values of U . For a fixed U , the broadening of the DP resonance changes linearly with fraction of impurities,^{39,40} as we have also obtained in the case of the vacancy defects (see Fig. 3). Larger $|U|$ in this situation leads to a larger slope of the $\Gamma_{\text{DP}}(\mathcal{C}_i)$ dependence. The same trend as for the shift of the plasmon frequency is observed: the negative U induces stronger change of the width of the DP resonance with \mathcal{C}_i . We attribute this effect to the impurity induced resonances in DOS above the Dirac point.^{11,33,45,46} As a consequence, the DOS $\rho(E_F)$ increases above the value predicted by the perturbation theory, and new plasmon decay channels become possible.¹⁰ It is worth noting that the shift of the Fermi level energy with respect to the Dirac point, $E_F \rightarrow E_F - \mathcal{C}_i U$, might also affect the plasmon decay by changing the energies of the inter-band transitions involving the π bands of graphene and the defect (impurities and nanostructure boundary) induced states. Further work is needed to determine the precise role of various mechanisms in the dependence of Γ_{DP} on U and \mathcal{C}_i .

To further quantify the effect of the impurities, we show in Figure 5d the maximum absorption cross section calculated at ω_{DP} resonance frequency as function of \mathcal{C}_i . The defect and impurity-induced broadening of the DP resonance leads in the present case to a strong

sensitivity of the optical response to a low fraction of substitutional impurities. We obtain more than 17% reduction of the maximum absorption cross section for the $\mathcal{C}_i = 0.004$ fraction of the $U = \pm 3$ eV substitutional impurities representative for the Nitrogen and Boron.^{31,33}

Conclusions

Using the time-dependent tight-binding approach we have studied the effect of the missing atom vacancies and substitutional impurities on the plasmon resonance in the optical absorption spectra of small graphene nanoflakes. As representative examples, we considered electrostatically doped nanoflakes of circular and triangular geometry. Our work thus extends the earlier studies of graphene plasmon scattering on extended defects^{38,47} to the case of even smaller, atomic scale, defects of graphene lattice.

Inline with available empirical information, we demonstrate that the dipolar plasmon mode of graphene nanoflakes is extremely sensitive to the atomic scale defects of graphene lattice. E.g. 0.5% of vacancies can fully quench the plasmon resonance of the absorption spectra because of the reduction of the optical conductivity associated with electron scattering on defects and because of the plasmon decay into the electron-hole pair excitations involving the defect-induced electronic states.

We have found that, along with broadening of the plasmon resonance, the lattice vacancies or substitutional impurities lead to the red- or blue- shift of the dipolar plasmon frequency (depending on the nature of the defect) at fixed energy of the Fermi level. This can be explained as a result of the modification of the density of electronic states at the Fermi level of graphene.

At low fractions of defects \mathcal{C}_i we obtained that both the broadening and the frequency shift of the plasmon line show a linear dependence on \mathcal{C}_i particularly well seen in the case of the substitutional impurities. This result can be consistently explained using the Drude model of the optical conductivity of graphene, and accounting for the impurity-induced

modification of its electronic structure and of the electron collision time, as reported in detailed theoretical studies.

We believe that results reported in this study will contribute to the understanding of the factors controlling the plasmon modes of graphene nanoflakes in realistic conditions, thus facilitating the transfer from the laboratory studies to technological applications.

Supporting Information Available

The following files are available free of charge. Supporting Information providing

- Derivation of Equation 10;
- Comparison between the analytical model and the TDTB results for the plasmon energy shift;
- Analysis of the effect of the substitutional donor impurities on the DP resonance of the free-standing nanoflake.

References

- (1) Geim, A. K.; Novoselov, K. S. The rise of graphene. *Nature Materials* **2007**, *6*, 183–191.
- (2) Basov, D. N.; Fogler, M. M.; García de Abajo, F. J. Polaritons in van der Waals materials. *Science* **2016**, *354*.
- (3) Castro Neto, A. H.; Guinea, F.; Peres, N. M. R.; Novoselov, K. S.; Geim, A. K. The electronic properties of graphene. *Rev. Mod. Phys.* **2009**, *81*, 109–162.
- (4) García de Abajo, F. J. Graphene Plasmonics: Challenges and Opportunities. *ACS Photonics* **2014**, *1*, 135–152.

- (5) Low, T.; Avouris, P. Graphene Plasmonics for Terahertz to Mid-Infrared Applications. *ACS Nano* **2014**, *8*, 1086–1101, PMID: 24484181.
- (6) Das Sarma, S.; Adam, S.; Hwang, E. H.; Rossi, E. Electronic transport in two-dimensional graphene. *Rev. Mod. Phys.* **2011**, *83*, 407–470.
- (7) Kotov, V. N.; Uchoa, B.; Pereira, V. M.; Guinea, F.; Castro Neto, A. H. Electron-Electron Interactions in Graphene: Current Status and Perspectives. *Rev. Mod. Phys.* **2012**, *84*, 1067–1125.
- (8) Yan, H.; Low, T.; Zhu, W.; Wu, Y.; Freitag, M.; Li, X.; Guinea, F.; Avouris, P.; Xia, F. Damping pathways of mid infrared plasmons in graphene nanostructures. *Nature Photonics* **2013**, *7*, 394–399.
- (9) Chen, J.-H.; Cullen, W. G.; Jang, C.; Fuhrer, M. S.; Williams, E. D. Defect Scattering in Graphene. *Phys. Rev. Lett.* **2009**, *102*, 236805.
- (10) Viola, G.; Wenger, T.; Kinaret, J.; Fogelström, M. Graphene plasmons: Impurities and nonlocal effects. *Phys. Rev. B* **2018**, *97*, 085429.
- (11) Pereira, V. M.; Lopes dos Santos, J. M. B.; Castro Neto, A. H. Modeling disorder in graphene. *Phys. Rev. B* **2008**, *77*, 115109.
- (12) Yuan, S.; De Raedt, H.; Katsnelson, M. I. Modeling electronic structure and transport properties of graphene with resonant scattering centers. *Phys. Rev. B* **2010**, *82*, 115448.
- (13) Wehling, T. O.; Yuan, S.; Lichtenstein, A. I.; Geim, A. K.; Katsnelson, M. I. Resonant Scattering by Realistic Impurities in Graphene. *Phys. Rev. Lett.* **2010**, *105*, 056802.
- (14) Stauber, T.; Peres, N. M. R.; Guinea, F. Electronic transport in graphene: A semiclassical approach including midgap states. *Phys. Rev. B* **2007**, *76*, 205423.

- (15) Kaasbjerg, K. Atomistic T -matrix theory of disordered two-dimensional materials: Bound states, spectral properties, quasiparticle scattering, and transport. *Phys. Rev. B* **2020**, *101*, 045433.
- (16) Jablan, M.; Buljan, H.; Soljačić, M. Plasmonics in graphene at infrared frequencies. *Phys. Rev. B* **2009**, *80*, 245435.
- (17) Sule, N.; Willis, K. J.; Hagness, S. C.; Knezevic, I. Terahertz-frequency electronic transport in graphene. *Phys. Rev. B* **2014**, *90*, 045431.
- (18) Thongrattanasiri, S.; Manjavacas, A.; García de Abajo, F. J. Quantum Finite-Size Effects in Graphene Plasmons. *ACS Nano* **2012**, *6*, 1766–1775.
- (19) Lewandowski, C.; Levitov, L. Intrinsically undamped plasmon modes in narrow electron bands. *Proceedings of the National Academy of Sciences* **2019**, *116*, 20869–20874.
- (20) Langer, T.; Baringhaus, J.; Pfnür, H.; Schumacher, H. W.; Tegenkamp, C. Plasmon damping below the Landau regime the role of defects in epitaxial graphene. *New Journal of Physics* **2010**, *12*, 033017.
- (21) Panchakarla, L. S.; Subrahmanyam, K. S.; Saha, S. K.; Govindaraj, A.; Krishnamurthy, H. R.; Waghmare, U. V.; Rao, C. N. R. Synthesis, Structure, and Properties of Boron- and Nitrogen-Doped Graphene. *Advanced Materials* **2009**, *21*, 4726–4730.
- (22) Araujo, P. T.; Terrones, M.; Dresselhaus, M. S. Defects and impurities in graphene-like materials. *Materials Today* **2012**, *15*, 98–109.
- (23) Han, W.; Kawakami, R. K.; Gmitra, M.; Fabian, J. Graphene spintronics. *Nature Nanotechnology* **2014**, *9*, 794–807.
- (24) Cox, J. D.; Silveiro, I.; García de Abajo, F. J. Quantum Effects in the Nonlinear Response of Graphene Plasmons. *ACS Nano* **2016**, *10*, 1995–2003, PMID: 26718484.

- (25) Aguilon, F.; Marinica, D. C.; Borisov, A. G. Molecule Detection with Graphene Dimer Nanoantennas. *The Journal of Physical Chemistry C* **2020**, *124*, 28210–28219.
- (26) Hwang, E. H.; Adam, S.; Sarma, S. D. Carrier Transport in Two-Dimensional Graphene Layers. *Phys. Rev. Lett.* **2007**, *98*, 186806.
- (27) Yuan, S.; Roldán, R.; De Raedt, H.; Katsnelson, M. I. Optical conductivity of disordered graphene beyond the Dirac cone approximation. *Phys. Rev. B* **2011**, *84*, 195418.
- (28) Novko, D. Dopant Induced Plasmon Decay in Graphene. *Nano Letters* **2017**, *17*, 6991–6996, PMID: 28972379.
- (29) Pereira, V. M.; Guinea, F.; Lopes dos Santos, J. M. B.; Peres, N. M. R.; Castro Neto, A. H. Disorder Induced Localized States in Graphene. *Phys. Rev. Lett.* **2006**, *96*, 036801.
- (30) Banhart, F.; Kotakoski, J.; Krasheninnikov, A. V. Structural Defects in Graphene. *ACS Nano* **2011**, *5*, 26–41, PMID: 21090760.
- (31) Pedersen, T. G.; Pedersen, J. G. Self-consistent tight-binding model of B and N doping in graphene. *Phys. Rev. B* **2013**, *87*, 155433.
- (32) Wehling, T.; Katsnelson, M.; Lichtenstein, A. Adsorbates on graphene: Impurity states and electron scattering. *Chemical Physics Letters* **2009**, *476*, 125–134.
- (33) Tison, Y.; Lagoute, J.; Repain, V.; Chacon, C.; Girard, Y.; Rousset, S.; Joucken, F.; Sharma, D.; Henrard, L.; Amara, H.; Ghedjatti, A.; Ducastelle, F. Electronic Interaction between Nitrogen Atoms in Doped Graphene. *ACS Nano* **2015**, *9*, 670–678, PMID: 25558891.
- (34) Grigorenko, A. N.; Polini, M.; Novoselov, K. S. Graphene plasmonics. *Nature Photonics* **2012**, *6*, 749–758.

- (35) Fang, Z.; Thongrattanasiri, S.; Schlather, A.; Liu, Z.; Ma, L.; Wang, Y.; Ajayan, P. M.; Nordlander, P.; Halas, N. J.; García de Abajo, F. J. Gated Tunability and Hybridization of Localized Plasmons in Nanostructured Graphene. *ACS Nano* **2013**, *7*, 2388–2395, PMID: 23390960.
- (36) García de Abajo, F. J. Multiple Excitation of Confined Graphene Plasmons by Single Free Electrons. *ACS Nano* **2013**, *7*, 11409–11419.
- (37) Yu, R.; Cox, J. D.; de Abajo, F. J. G. Nonlinear Plasmonic Sensing with Nanographene. *Phys. Rev. Lett.* **2016**, *117*, 123904.
- (38) Chen, J.; Nesterov, M. L.; Nikitin, A. Y.; Thongrattanasiri, S.; Alonso-González, P.; Slipchenko, T. M.; Speck, F.; Ostler, M.; Seyller, T.; Crassee, I.; Koppens, F. H. L.; Martin-Moreno, L.; García de Abajo, F. J.; Kuzmenko, A. B.; Hillenbrand, R. Strong Plasmon Reflection at Nanometer-Size Gaps in Monolayer Graphene on SiC. *Nano Letters* **2013**, *13*, 6210–6215, PMID: 24188400.
- (39) Principi, A.; Vignale, G.; Carrega, M.; Polini, M. Impact of disorder on Dirac plasmon losses. *Phys. Rev. B* **2013**, *88*, 121405.
- (40) Jablan, M.; Soljačić, M.; Buljan, H. Effects of screening on the optical absorption in graphene and in metallic monolayers. *Phys. Rev. B* **2014**, *89*, 085415.
- (41) Yannouleas, C.; Vigezzi, E.; Broglia, R. A. Evolution of the optical properties of alkali-metal microclusters towards the bulk: The matrix random-phase-approximation description. *Phys. Rev. B* **1993**, *47*, 9849–9861.
- (42) Varas, A.; García-González, P.; Feist, J.; García-Vidal, F.; Rubio, A. Quantum plasmonics: From jellium models to ab initio calculations. *Nanophotonics* **2016**, *5*, 409–426.
- (43) Ukhtary, M. S.; Saito, R. Surface plasmons in graphene and carbon nanotubes. *Carbon* **2020**, *167*, 455–474.

- (44) Ariasoca, T. A.; Sholihun,; Santoso, I. Trotter-Suzuki-time propagation method for calculating the density of states of disordered graphene. *Computational Materials Science* **2019**, *156*, 434–440.
- (45) Wu, S.; Jing, L.; Li, Q.; Shi, Q. W.; Chen, J.; Su, H.; Wang, X.; Yang, J. Average density of states in disordered graphene systems. *Phys. Rev. B* **2008**, *77*, 195411.
- (46) Nanda, B. R. K.; Sherafati, M.; Popović, Z. S.; Satpathy, S. Electronic structure of the substitutional vacancy in graphene: density-functional and Green's function studies. *New Journal of Physics* **2012**, *14*, 083004.
- (47) Slipchenko, T. M.; Nesterov, M. L.; Hillenbrand, R.; Nikitin, A. Y.; Martín-Moreno, L. Graphene Plasmon Reflection by Corrugations. *ACS Photonics* **2017**, *4*, 3081–3088.

TOC Graphic

